A 3D electron fluid model with energy balance for plasma plumes

IEPC-2022-321

Presented at the 37th International Electric Propulsion Conference
Massachusetts Institute of Technology, Cambridge, MA, USA
June 19-23, 2022

Alberto Modesti[1] and Jiewei Zhou[2] and Eduardo Ahedo[3]
Equipo de Propulsión Espacial y Plasmas (EP2), Universidad Carlos III de Madrid, Leganés, Spain

Filippo Cichoki[4]
Istituto per la Scienza e Tecnologia dei Plasmi, Bari, Italy

EP2PLUS is a 3D hybrid simulation code designed to analyze the expansion of energetic plasma plumes and its interaction with nearby objects, which is a subject of high interest. Heavy species are treated with a particle-in-cell formulation while a fluid model is used for electrons. The electron model is able to deal with moderate magnetic field but the momentum equation is closed with a polytropic relation for the electron temperature. This is inadequate for magnetized, mildly collisional regions of the plume. This paper presents work in progress to add the electron energy equation to the model with a Fourier's closure law for the heat flux. An example with a magnetically-guided plume shows the differences between the two approaches.

I. Introduction

Electric thrusters produce high-energy plasma plumes, which are important in completing the thrust generation process but they lead to potentially damaging interaction (electric charging and mechanical erosion/contamination) with surrounding surfaces (solar arrays, equipment, antennas...) [1, 2]. Nonetheless, on the other end, plasma plumes have also been proposed as part of an attractive deorbiting technique for space debris [3, 4].

The characterization of plasma thruster plumes is challenging due to their rarefied conditions (away from local thermodynamic equilibrium) and the huge difference between the dynamics of the heavy/accelerated ions and the light/confined electrons. Plasma plumes of Gridded Ion Thrusters (GITs) are unmagnetized, but those of Hall Effect Thrusters (HETs) and Electrodeless Plasma Thrusters (EPTs) are magnetized for electrons, leading to highly anisotropic (and complex) dynamics for them [5, 6]. In addition and in spite of thruster channels being usually axisymmetric, plasma plumes are often 3D due to the presence of lateral cathodes as neutralizers (as in GITs and HETs), thrust vectoring elements [7], other surrounding surfaces, or just the presence of the uniform geomagnetic field [8].

Numerical modeling of plasma plumes can be either kinetic, fluid or hybrid. Currently, even in the context of massive computing, hybrid modeling is the best trade-off between physical reliability and detailed results in 2D and 3D scenarios. Reference [3] presents EP2PLUS, a 3D hybrid code for plasma plumes, which adopts a particle-in-cell (PIC) formulation for heavy species and a magnetized fluid formulation for electrons. It was originally created to simulate quasineutral, current-free plumes, and their interaction with surrounding objects and surfaces [4]. Recently EP2PLUS has been used to determine: the 3D structure of an initially axisymmetric plume under the influence of an oblique geomagnetic field [8]; the 3D neutralizer effects in a HET plume [9]; and the neutralization of electric charge and current in a GIT plume [10].

The most challenging part in EP2PLUS and other hybrid codes [11, 12] is the fluid model for magnetized electrons. In the weakly-collisional scenario, there are uncertainties in central terms of the fluid equations, such as the pressure

[1]PhD Candidate, Bioengineering and Aerospace Engineering Department, amodesti@pa.uc3m.es.
[2]Assistant professor, Bioengineering and Aerospace Engineering Department, jiewei.zhou@uc3m.es.
[3]Full professor, Bioengineering and Aerospace Engineering Department, eduardo.ahedo@uc3m.es.
[4]Senior post-doc researcher, Istituto per la Scienza e Tecnologia dei Plasmi, filippo.cichocki@istp.cnr.it.

tensor and the heat flux vector. Besides, high-frequency instabilities introduce 'anomalous' terms in the slow-dynamics equations for electron transport [13–15].

EP2PLUS assumes an isotropic pressure tensor and introduces wave-based anomalous transport empirically as an additional collisional effect, which is within the state-of-art. The main limitation of the code is to avoid the energy equation by closing the set of fluid equations with a polytropic state law for the pressure (i.e. the temperature), which implies that the plume cools down proportionally to its rarefaction. There exists partial empirical validation of this polytropic closure in far plumes, preferably unmagnetized [12].

However, that closure is not expected to apply in near-plumes, where collisional, electric, and magnetic events are relevant. This is for instance the case of the very active near-plume of a HET. This has been demonstrated in Ref. [9] where EP2PLUS 3D polytropic simulations were compared against a 2D code considering the full energy balance. EP2PLUS was very satisfactory in reproducing the 3D ion and electron currents developing in the HET near plume but yielded erroneous temperature and electric potential maps.

This paper reports on the advances in implementing a full electron energy equation to EP2PLUS within the electron model. Thus, the model is closed at the level of the heat flux vector, where an anisotropic Fourier´s diffusive law is proposed, as suggested by both kinetic and experimental studies for non-equilibrium thermodynamic conditions [16–18].

The paper is structured as follows. Section II describes the hybrid model in EP2PLUS, with detailed insight into its 3D electron fluid model and its numerical treatment. Section III.A discusses the simulation setup. Section III.B discusses the simulation results with focus on the energy balance outputs and the consistency of the implementation. Section IV summarizes the conclusions and outlines future works.

II. The full electron fluid model

The code EP2PLUS is presented with much detail in Ref. [3] and features two main modules, the Ion one with the PIC formulation for all heavy species and the Electron one with the fluid formulation. The two modules are run sequentially and the same spatial mesh is used for the two modules, which avoids interpolation errors on plasma magnitudes. In the following, however, only the extended fluid model is described.

The set of fluid equations for electrons in a quasineutral plume is

$$n_e = \sum_s Z_s n_s \tag{1}$$

$$\nabla \cdot \boldsymbol{j}_e = -\nabla \cdot \boldsymbol{j}_i + S_c, \tag{2}$$

$$\boldsymbol{j}_e = \bar{\bar{\mu}}_e \cdot \left(-en_e\nabla\phi + \nabla p_e - \boldsymbol{F}_{ch}\right), \tag{3}$$

$$\nabla \cdot \boldsymbol{P}_e'' = \boldsymbol{j}_e \cdot \boldsymbol{E} + Q_c - \frac{3}{2}\frac{\partial p_e}{\partial t}. \tag{4}$$

$$\boldsymbol{P}_e'' = \frac{5}{2} T_e n_e \Big(\boldsymbol{u}_e - \bar{\bar{\mu}}_e \cdot \nabla(T_e/e)\Big). \tag{5}$$

Equation (1) is the quasineutrality condition for the electron density n_e. In the right side, s represents each of the heavy species with charge number Z_s. The Ion module of the code provides the species density n_s, the particle flux $\boldsymbol{g}_s \equiv n_s \boldsymbol{u}_s$, and other higher-order magnitudes. Equation (2) is the current conservation equation, where $\boldsymbol{j}_e = -en_e\boldsymbol{u}_e$ and $\boldsymbol{j}_i = \sum_s eZ_s\boldsymbol{g}_s$ are the electron and ion current densities, and S_c represents any volumetric source of electric current (such as the cathode electron source in some HET models [19]).

Equation (3) is the Ohm's law, obtained from the inertialess limit of the electron momentum equation. There, ϕ is the electric potential, $p_e = n_e T_e$ is the electron scalar pressure, and

$$\bar{\bar{\mu}}_e = \mu_e \begin{pmatrix} 1 & \chi b_z & -\chi b_y \\ -\chi b_z & 1 & \chi b_x \\ \chi b_y & -\chi b_x & 1 \end{pmatrix}^{-1} \tag{6}$$

is the mobility tensor, with $\mu_e = e/m_e\nu_e$ the scalar mobility, $\chi = \omega_{ce}/\nu_e \equiv B\mu_e$ the Hall parameter ($\omega_{ce} = eB/m_e$ is the electron gyrofrequency), and $(b_x, b_y, b_z) = \boldsymbol{B}/B \equiv \boldsymbol{1}_\parallel$ the magnetic unit vector in the Cartesian reference frame. The collisional force on electrons with heavy species is expressed, in the electron momentum equation, as

$\boldsymbol{F}_c = -m_e n_e \sum_s \nu_{es}(\boldsymbol{u}_e - \boldsymbol{u}_s)$ with ν_{es} the corresponding collision frequencies with heavy species s. This gives rise to the term $\boldsymbol{F}_{ch} = m_e n_e \sum_s \nu_{es}\boldsymbol{u}_s$ in Eq. (3). The total collision frequency in this equation is

$$\nu_e = \sum_s \nu_{es} + \alpha_a \omega_{ce} \tag{7}$$

where the last term corresponds to the wave-based anomalous transport, with α_a a fitting parameter.

Equation (4) is the energy equation in the inertialess limit for the energy flux vector $\boldsymbol{P}_e''$. The right side includes the work of the electric field $\boldsymbol{E} = -\nabla\phi$, the term Q_c accounting for collisional events, and the temporal derivative of the electron energy density. Equation (5) closes the fluid model with a convective-diffusive closure for the energy flux vector: in the right side, the first term is the enthalpy flux and the second term is the heat flux, which follows here an anisotropic diffusive law. This Fourier-type closure is the 3rd-moment fluid equation and represents the chosen alternative to the polytropic closure 2nd-moment fluid equation.

A. Boundary conditions

Since Eq. (1) yields the electron density, Eqs. (2)-(5) yield $(\phi, \boldsymbol{j}_e)$ and $(T_e, \boldsymbol{P}_e'')$. If $\boldsymbol{n}$ is the outward normal to a boundary point, conditions on $j_{ne} \equiv -en_e u_{ne} = \boldsymbol{j}_e \cdot \boldsymbol{n}$ and $P_{ne}'' = \boldsymbol{P}_e'' \cdot \boldsymbol{n}$ are needed (other variables along $\boldsymbol{n}$ are defined in the same way). If the plasma is quasineutral, boundary conditions are imposed at the sheath edge, and not directly at the walls.

For a dielectric wall, let: $\phi_{WQ} = \phi_Q - \phi_W$ be the sheath potential drop between Q and the wall point W; δ_r be the fraction of primary electrons reflected back elastically at the wall; δ_s be the ratio between true secondary emission flux from the wall and the primary electron flux to the wall; and σ_{rp} be the replenishment factor of the Maxwellian VDF tail of collected primary electrons, equal to 1 for full replenishment. The zero-current condition

$$j_{ne} = -j_{ni} \tag{8}$$

yields the electron current desnity. Since the sheath solution states that

$$j_{ne} = (1-\delta_s)(1-\delta_r)\sigma_{rp} e n_{eQ} \sqrt{\frac{T_{eQ}}{2\pi m_e}} \exp\left(\frac{-e\phi_{WQ}}{T_{eQ}}\right). \tag{9}$$

the potential fall in the sheath is obtained from

$$\frac{e\phi_{WQ}}{T_{eQ}} = \ln\sqrt{\frac{m_i}{2\pi m_e}} + \ln[(1-\delta_r)(1-\delta_s)\sigma_{rp}] - \ln\left(\frac{j_{ni}}{en_{eQ}}\sqrt{\frac{m_i}{T_{eQ}}}\right) \tag{10}$$

Finally, the electron energy flux at the sheath edge is

$$P_{neQ}'' \simeq (-j_{ne})\left[\frac{2T_{eQ}}{e(1-\delta_s)} + \phi_{WQ}\right]. \tag{11}$$

For a metallic wall A driving a current I_A, the wall potential ϕ_A is constant and is obtained from the implicit integral equation

$$I_A(\phi_A) = \int_{\partial S_B} dS[j_{ni} + j_{ne}(\phi_A)] \tag{12}$$

with $j_{ne}(\phi_A)$ satisfying (9) (exchanging W and Q by A and B). The domain of the integral is the surface ∂S_B of the sheath edge B of the wall, and we are assuming a normal sheath with $\phi_{AB} = \phi_B - \phi_A > 0$. The local electron energy flux at B satisfies (11), again exchanging W and Q by A and B. For the range of energies in plasma thruster plumes, the SEE of metallic surfaces is negligible; in fact we will take $\delta_s = 0$ and $\delta_r = 0$.

The plasma plume is considered current-free. For the present state of development of the model, boundary conditions at the finite-size simulated plumes are *local*, and formally equivalent to a dielectric wall, or *global*, and formally equivalent to a metallic wall driving no net current. This second alternative is more complex to implement but more realistic both for a plume expansion into a vacuum chamber or in free space. In this second case, the 'sheath' between the simulated boundary and the 'wall' can be interpreted as a 'downstream matching layer' to infinity [20].

B. Further discussion

Several important observations on the fluid model are worth before addressing the simulations. First, in a magnetized scenario (i.e. $\chi \gg 1$), $\bar{\bar{\mu}}_e$ is highly anisotropic, and as a result, the derivatives along the magnetic lines, $\nabla_\parallel$, yield

$$en_e\nabla_\parallel\phi \approx T_e\nabla_\parallel n_e \gg n_e\nabla_\parallel T_e, \mu_e^{-1} j_{\parallel e} \tag{13}$$

which hampers the numerical computation of the parallel current $j_{\parallel e}$, a subdominant term in Eq. (3). A proven way to mitigate numerically this is the use of the thermalized potential [19, 21, 22]

$$\Phi = \phi - \frac{T_e}{e}\ln\frac{n_e}{n_0}, \qquad \text{i.e.} \qquad n_e = n_0 \exp\left(e\frac{(\phi-\Phi)}{T_e}\right), \tag{14}$$

with n_0 a convenient reference value; notice that Φ also measures the deviation of the electric potential from a Boltzmann relation. Then Eq. (3) becomes

$$\boldsymbol{j}_e = \bar{\bar{\mu}}_e \cdot \Big[-en_e\nabla\Phi - n_e\big(\ln\frac{n_e}{n_0}+1\big)\nabla T_e - \boldsymbol{F}_{ch}\Big], \tag{15}$$

The first force of the right hand side ($-en_e\nabla\Phi$) is now the combination of the (opposed) electric and density-gradient forces.

The second observation is that by applying $-\boldsymbol{j}_e \cdot \nabla\phi = -\nabla \cdot \phi \boldsymbol{j}_e + \phi\nabla \cdot \boldsymbol{j}_e$ and using the current conservation equation, the energy equation (4) can be expressed as

$$\nabla \cdot (\boldsymbol{P}_e'' - e\phi n_e \boldsymbol{u}_e) = (-\nabla \cdot j_i + S_c)\phi + Q_c - \frac{3}{2}\frac{\partial p_e}{\partial t}. \tag{16}$$

In the sourceless, stationary, collisionless limit (not unusual for plasma plumes) the right side is zero, implying that the total electron energy (including the electric potential contribution) is conserved.

Third, this last equation allows us to unveil when the full electron model reduces to the polytropic closure used so far in EP2PLUS. Two are the conditions to be satisfied: first, a sourceless, stationary, collisionless plume; and second, a convective behavior of the heat flux vector instead of a diffusive one, that is

$$\boldsymbol{P}_e'' = \frac{5}{2}T_e n_e \boldsymbol{u}_e + \alpha_q T_e n_e \boldsymbol{u}_e. \tag{17}$$

instead of (5). Then, calling

$$\gamma = \frac{5+2\alpha_q}{3+2\alpha_q} \tag{18}$$

and after some algebra on the electron fluid equations, one gets a polytropic equation of state along the electron streamlines,

$$(\boldsymbol{u}_e \cdot \nabla)\ln(p_e/n_e^\gamma) = 0, \tag{19}$$

which yields p_e/n_e^γ =const if conditions are uniform upstream. Therefore, the polytropic closure requires, beyond no collisions, different physics for the heat flux. It must be added that a convective behavior of the heat flux in collisionless scenarios have been found in some collisionless scenarios [23, 24] although it could be limited to the component parallel to a magnetic field [25, 26]. Indeed, a central difference between the heat flux in (17) and (5) is that the first one is isotropic and the second one anisotropic.

In non neutral subregions of the plume, Eqs. (1) and (2) are substituted by

$$n_e = n_i + (\epsilon_0/e)\nabla^2\phi, \tag{20}$$

$$\nabla \cdot \boldsymbol{j}_e = -\nabla \cdot \boldsymbol{j}_i + S_c + \partial\rho_{el}/\partial t, \tag{21}$$

and a Poisson's solver is needed for the first one. Ref. [3] explains how this is achieved in EP2PLUS.

C. Numerical treatment

The electron fluid equations are solved in a structured staggered mesh. The equations for current conservation and electron energy are solved for $\boldsymbol{j}_e$ and $\boldsymbol{P}_e''$ applying a Finite Volumes Method on each cell. The equations relating these two vector variables with the gradients of ϕ (or Φ) and T_e are solved with a Finite Difference Method. This discretization provides linear matrix relations for ϕ and T_e at the cell centers and for the perpendicular components of $\boldsymbol{j}_e$ and $\boldsymbol{P}_e''$ at the cell faces centers.

III. Numerical simulations

A. Physical and numerical setup

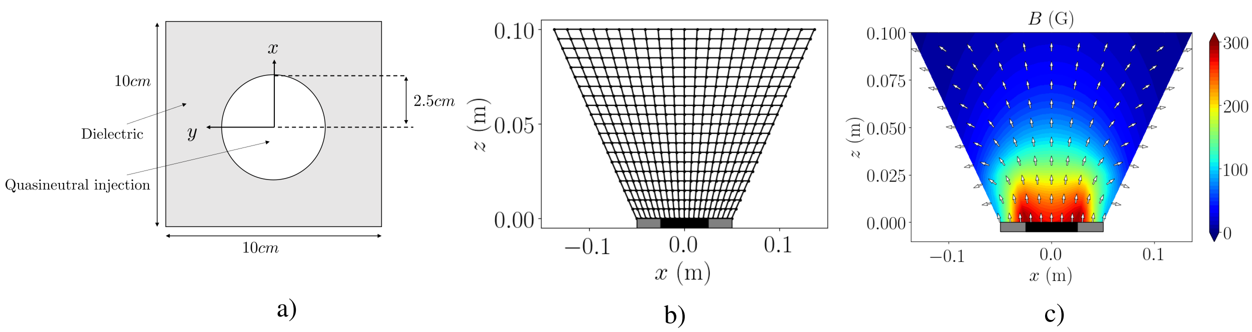

Fig. 1 (a) Sketch of the source exit (at $z = 0$), (b) employed mesh, and (c) magnetic field on the $y = 0$ plane. The injection and the dielectric surfaces are highlighted by respectively black and grey rectangles.

The test case simulated here consists of a magnetized quasineutral plume expansion. This scenario was already simulated (with different physical and numerical setup) by the 2D axisymmetric code HYPHEN [12], featuring the full energy equation, and also by the same EP2PLUS [27], with a polytropic closure.

Figure 1 shows the sketch of the simulated case. Panel (a)-(b) show the plume domain with the source exit located at $z = 0$, consisting of a circular injector surface of radius 0.025m, surrounded by a dielectric surface. The simulated domain is rectangular, with dimensions of 0.1x0.1m at $z = 0$ and then it expands conically downstream, with dimensions of 0.28x0.28m. The mesh used is Cartesian and non-uniform, with 20x20x20 cells, adapted to the conical domain. The time step to advance ions is $5 \cdot 10^{-7}$s and the total simulated time is 1ms.

The propellant is Xenon, and we inject a Xe+ and Xe flows of 4.5mg/s and 0.5mg/s, respectively, both following Parks-Katz self-similar radial profiles [28]. The simulated species are the injected fast ions and slow neutrals, plus fast neutrals and slow ions coming from charge exchange (CEX) collisions. Panel (c) shows the magnetic field, which is an axially divergent magnetic field, a magnetic nozzle configuration, and with a maximum value of 300G. Anomalous electron transport is included adding an anomalous collision frequency $\alpha_a \omega_{ce}$ with $\alpha_a = 0.1$. Indeed, this makes this phenomenon dominant and the Hall parameter is $\chi \approx \alpha_a^{-1}$, which has the advantage of controlling χ easily.

Some simplifications taken in the simulation and affecting Eq. 4 are the following: no inelastic collisions are being simulated, so $Q_c = 0$; and, since a steady state solution is looked for, temporal derivatives of electron energy are disregarded, so $\partial p_e / \partial t = 0$.

Finally, the boundary conditions have to be specified for this simulation case. At the dielectric walls, null local net current conditions are considered, $j_{ne} = -j_{ni}$, while the heat flux is given by the sheath model described in Section II.A with no SEE emission. At the injection surface, local current ambipolarity is assumed, together with a given temperature profile starting from an assumed maximum T_{e0} at the center of the injection surface (here 8eV) and with an exponential decay (until values of 4.8eV at the injection surface edges). At the free loss surface, local current ambipolarity, and an electron energy flux $P''_{ne} = cT_e n_e u_{ne}$ with $c = 4.5$ are assumed. This 'local' condition does not provide a information about the expansion to the infinity, but it is used for this test simulation since the 'global' condition is still being tested in EP2PLUS. In any case, Reference [12] shows that 'local' condition is robust and give consistent results.

Table 1 Simulation parameters.

Simulation parameters	Units	Values
PIC time-step	s	$5{\cdot}10^{-7}$
Simulation duration	s	$1{\cdot}10^{-3}$
Number of mesh cells	-	$20 \times 20 \times 20$
Simulated species	-	Fast ions, slow neutrals (injection) Slow ions, fast neutrals (CEX)
Injection surface radius	m	0.025
Injection profiles	-	SSM
Ion injection mass flow	mg/s	4.5
Ion injection velocity	m/s	2800
Ion injection temperature	eV	0.05
Neutral injection mass flow	mg/s	0.5
Neutral injection velocity	m/s	300
Neutral injection temperature	eV	0.05
Electron injection maximum temperature	eV	8.0
Anomalous transport coefficient α_a	-	0.1
Maximum magnetic field strength	G	300

B. Simulation results

Figures 2 show the 2D maps on the $y = 0$ plane, for the relevant plasma magnitudes. Panel (a) and (e) are outputs from the PIC model, while the other panels are outputs of the fluid model. Panel (b) and (h) are outputs of the electron energy balance.

The electron temperature [panel (b)] features a cooling, which is expected from the kinetic and experimental studies [11, 18]. According to the Fourier's law of heat flux with anisotropic conductivity tensor, the temperature gradient is determined by the different electron mobility along and across the magnetic field [12]. Given the high mobility, the temperature is nearly isothermal along the magnetic field decaying 0.5-1eV downstream within the simulated plume extension. Given the low mobility, on the other hand, the decay is more noticeable across the magnetic field, about 3-4eV.

The plasma density [panel (a)] is maximum at the injection, about $10^{18}\mathrm{m}^{-3}$, and downstream it decays due to the expansion. The electric potential [panel (c)] drop, which transforms the thermal energy of the plasma into kinetic energy of ions, is approximately 50V, about 5 times the maximum electron temperature. Since unmagnetized, the ions [panel (e)] detach inwardly from the magnetic lines as expected [29]. The electrons [panel (d)], on the other hand, are confined and follow well the magnetic field lines. As result, the net current density [panel (f)] features no local current ambipolarity (i.e. $\tilde{\jmath} = 0$) despite the fact that the plasma beam is current free [30]. The plasma azimuthal currents, mainly due to the magnetized electrons [panel (g)], have a diamagnetic character, i.e. are opposite to the currents of the magnetic circuit generating the applied magnetic field, and are responsible for the confinement and the generation of magnetic thrust [31, 32]. Finally, the total energy flux [panel (h)] seems to follow well the electron current density bearing a mean energy of about P_{xze}/j_{xze} ~25-50eV in the main plume.

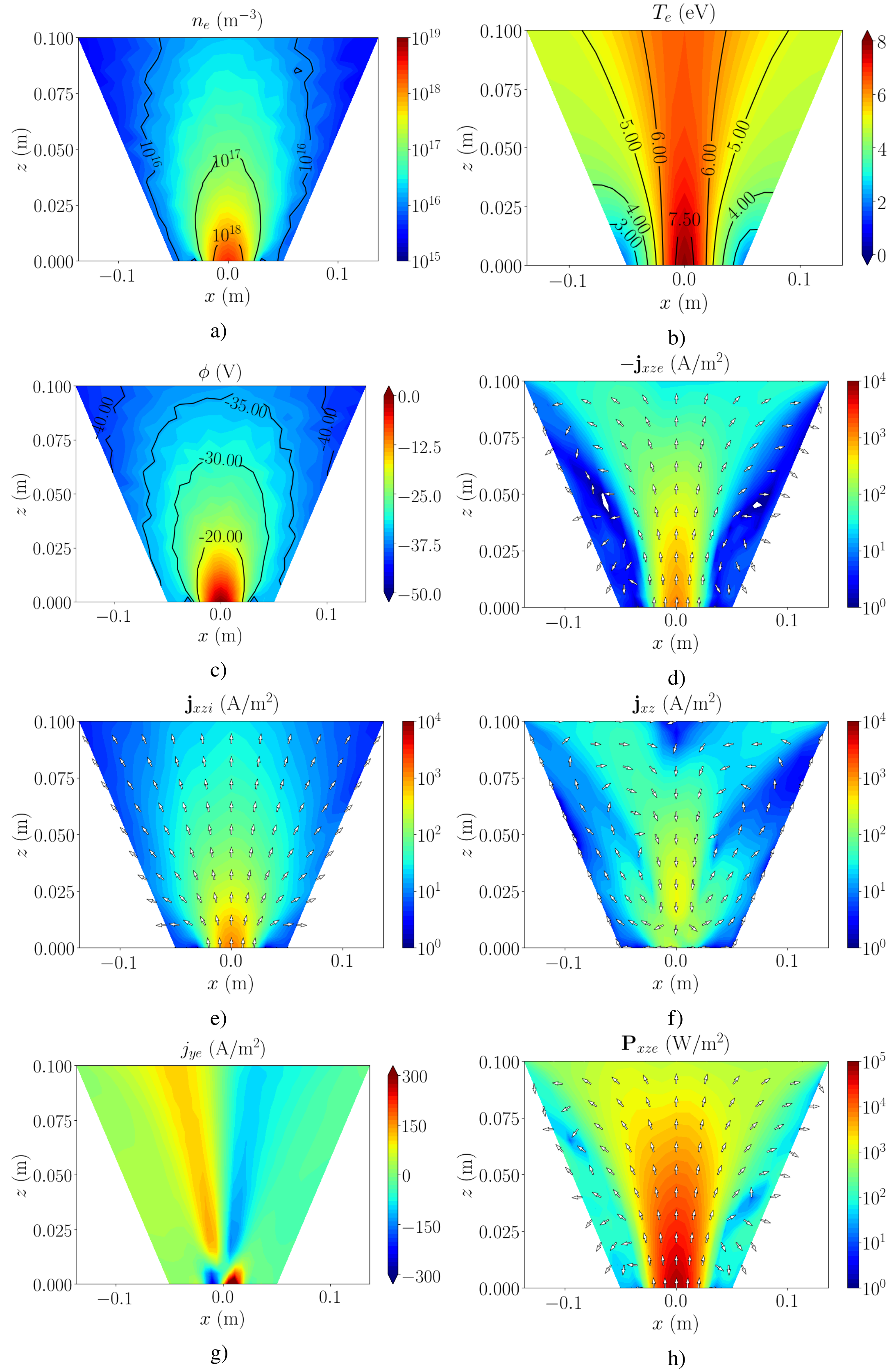

Fig. 2 2D maps of the main plasma magnitudes at the $y = 0$ plane.

C. Comparison with polytropic closure

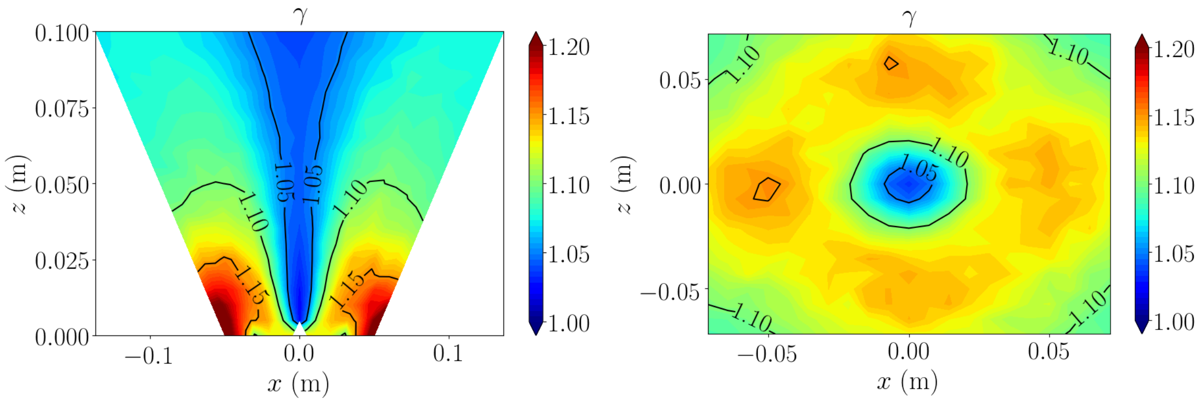

a) b)

Fig. 3 2D maps of the local polytropic coefficient at (left) $y = 0$ and (right) $z = 0.025$m.

Experimental [18, 33] and kinetic [25] studies suggest that a polytropic law, with a fitted polytropic coefficient,

$$\gamma = 1 + \frac{\ln T_e/T_{e0}}{\ln n_e/n_{e0}}, \tag{22}$$

matches well the electron cooling in the plume, being T_{e0} and n_{e0} referred to the thruster exit. Figure 3 shows the local polytropic coefficient for the simulation case here in order to have an idea of the deviation of the electron temperature here from EP2PLUS with the energy balance with respect to the polytropic one. Here, γ is not constant and its variation determines the deviation from the polytropic solution. Interestingly, it seems constant along the magnetic field lines, and varies across them, to values about 1.15-1.25 in the lateral plume. Thus, it seems to suggest that a polytropic closure can be used along a magnetic line but with different values of the coefficient for different lines. Indeed, most of the studies (the ones mentioned above for example) regarding the electron cooling are focused on paraxial expansion along the plume axis, and some recent experimental studies out of the plume axis suggested similar conclusions to those mentioned here [34].

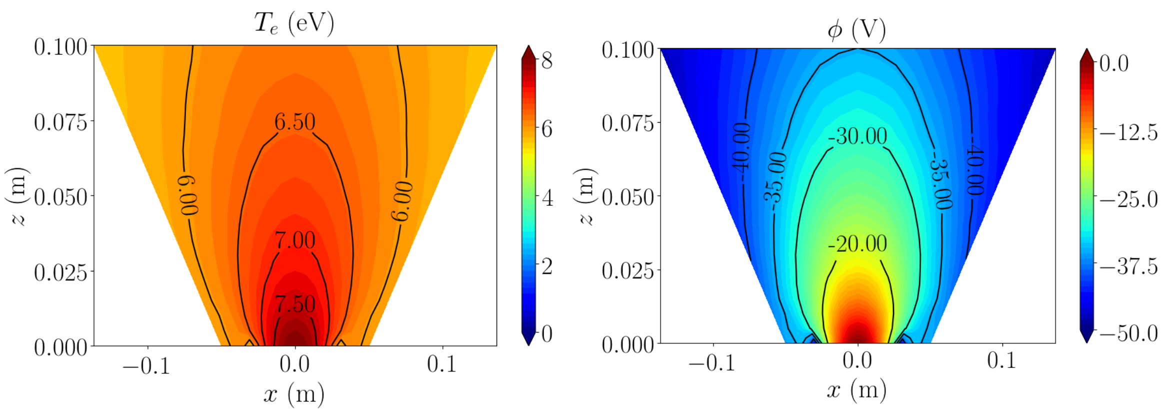

a) b)

Fig. 4 2D maps of plasma magnitudes at $y = 0$ for the old electron model, with the polytropic closure and $\gamma = 1.05$.

Figure 4 (a)-(b) shows, respectively, the 2D maps of electron temperature and potential for a simulation case where the closure of the electron fluid model is purely polytropic, and therefore a constant uniform γ is applied. Panel (a) shows that the cooling profile does not match the one obtained from the energy balance as expected. In this simplified closure, the reference point for the electron temperature in the polytropic law is the same, at the center of the injection surface, and the value is 8eV. The polytropic γ coefficient was tuned in order to match the temperature evolution along the plume axis obtained by solving the energy equation. This is a common approach adopted in simulations with a polytropic closure to compare with experiments as mentioned. The value found for γ in this case is 1.05 As a consequence, the cooling profile along the plume axis is nearly the same in simulations with energy equation and with a polytropic closure. On the other hand, along the other directions and especially across the magnetic field, the cooling profile has a different rate, and the reached temperature values are higher, about 2-3 eV higher in the polytropic closure case. Panel (b) (to be compared with Fig. 2 (c)) proves that the difference in the temperature induces differences in other plasma magnitudes, and in particular in the potential, which features a larger drop laterally in the polytropic case, in accordance with the higher predicted temperature.

IV. Conclusions

A 3D electron fluid model for a hybrid PIC-fluid code has been presented, which is weakly-collisional, diffusive and magnetized. Within the hybrid simulation code EP2PLUS, this can be applied to the simulation of the plasma plumes produced by different electric propulsion technologies. The implementation of the energy balance in the model constitutes an important upgrade of the code, which has been tested in a simulation of a magnetized plume, with a magnetic nozzle configuration typical of electrodeless plasma thrusters. Some results are shown to discuss the plasma discharge with a focus on the solution of the electron temperature from energy balance, and its deviation from the polytropic one.

Furthers studies should be focused on the application of the global conditions downstream, which provide a more realistic heat flux there, and on alternatives of the closure for the heat flux, for which kinetic and experimental studies suggest convective-type laws in the weakly-collisional limit.

Acknowledgments

All the numerical developments of this research have been supported by H2020-EU, under the project CHEOPS-MP (grant agreement ID: 101004226). The authors thank Pablo Fajardo, Mario Merino and Adrian Dominguez-Vazquez for support and counsel during the developments of this work.

References

[1] Garrett, H., "The charging of spacecraft surfaces," *Reviews of Geophysics*, Vol. 19, No. 4, 1981, pp. 577–616.

[2] Boyd, I., and Ketsdever, A., "Interactions between spacecraft and thruster plumes," *Journal of Spacecraft and Rockets*, Vol. 38, No. 3, 2001, p. 380.

[3] Cichocki, F., Domínguez-Vázquez, A., Merino, M., and Ahedo, E., "Hybrid 3D model for the interaction of plasma thruster plumes with nearby objects," *Plasma Sources Science and Technology*, Vol. 26, No. 12, 2017, p. 125008.

[4] Cichocki, F., Merino, M., and Ahedo, E., "Spacecraft-plasma-debris interaction in an ion beam shepherd mission," *Acta Astronautica*, Vol. 146, 2018, pp. 216–227. https://doi.org/10.1016/j.actaastro.2018.02.030.

[5] Ahedo, E., "Plasmas for space propulsion," *Plasma Physics and Controlled Fusion*, Vol. 53, No. 12, 2011, p. 124037. URL http://stacks.iop.org/0741-3335/53/i=12/a=124037.

[6] Kaganovich, I. D., Smolyakov, A., Raitses, Y., Ahedo, E., Mikellides, I. G., Jorns, B., Taccogna, F., Gueroult, R., Tsikata, S., Bourdon, A., Boeuf, J.-P., Keidar, M., Powis, A. T., Merino, M., Cappelli, M., Hara, K., Carlsson, J. A., Fisch, N. J., Chabert, P., Schweigert, I., Lafleur, T., Matyash, K., Khrabrov, A. V., Boswell, R. W., and Fruchtman, A., "Perspectives on Physics of ExB Discharges Relevant to Plasma Propulsion and Similar Technologies," *Physics of Plasmas*, Vol. 27, No. 12, 2020, p. 120601. https://doi.org/10.1063/5.0010135.

[7] Merino, M., and Ahedo, E., "Contactless steering of a plasma jet with a 3D magnetic nozzle," *Plasma Sources Science and Technology*, Vol. 26, No. 9, 2017, p. 095001. https://doi.org/10.1088/1361-6595/aa8061.

[8] Cichocki, F., Merino, M., and Ahedo, E., "Three-dimensional geomagnetic field effects on a plasma thruster plume expansion," *Acta Astronautica*, Vol. 175, 2020, pp. 190 – 203. https://doi.org/https://doi.org/10.1016/j.actaastro.2020.05.019.

[9] Cichocki, F., Domínguez-Vázquez, A., Merino, M., Fajardo, P., and Ahedo, E., "Three-dimensional neutralizer effects on a Hall-effect thruster near plume," *Acta Astronautica*, Vol. 187, 2021, pp. 498–510. https://doi.org/https://doi.org/10.1016/j.actaastro.2021.06.042, URL https://www.sciencedirect.com/science/article/pii/S0094576521003398.

[10] Perales-Díaz, J., Cichocki, F., Merino, M., and Ahedo, E., "Formation and neutralization of electric charge and current of an ion thruster plume," *Plasma Sources Science and Technology*, Vol. 30, No. 10, 2021, p. 105023. https://doi.org/10.1088/1361-6595/ac2a19.

[11] Zhou, J., Pérez-Grande, D., Fajardo, P., and Ahedo, E., "Numerical treatment of a magnetized electron fluid within an electromagnetic plasma thruster code," *Plasma Sources Science and Technology*, Vol. 28, No. 11, 2019, p. 115004.

[12] Zhou, A., J. Domínguez-Vazquez, Fajardo, P., and Ahedo, E., "Magnetized fluid electron model within a two-dimensional hybrid simulation code for electrodeless plasma thrusters," *Plasma Sources Science and Technology*, accepted for publication.

[13] Choueiri, E., "Plasma oscillations in Hall thrusters," *Physics of Plasmas*, Vol. 8, No. 4, 2001, pp. 1411–1426.

[14] Cavalier, J., Lemoine, N., Bonhomme, G., Tsikata, S., Honoré, C., and Grésillon, D., "Hall thruster plasma fluctuations identified as the ExB electron drift instability: Modeling and fitting on experimental data," *PoP*, Vol. 20, No. 8, 2013, p. 082107.

[15] Hepner, S., Wachs, B., and Jorns, B., "Wave-driven non-classical electron transport in a low temperature magnetically expanding plasma," *Applied Physics Letters*, Vol. 116, No. 26, 2020, p. 263502. https://doi.org/10.1063/5.0012668.

[16] Zhou, J., "Modeling and simulation of the plasma discharge in a radiofrequency thruster," Ph.D. thesis, Universidad Carlos III de Madrid, Leganés, Spain, 2021.

[17] Zawaideh, E., Kim, N., and Najmabadi, F., "Generalized parallel heat transport equations in collisional to weakly collisional plasmas," *The Physics of Fluids*, Vol. 31, 1988, pp. 3280–3285.

[18] Little, J., and Choueiri, E., "Electron Cooling in a Magnetically Expanding Plasma," *Physical Review Letters*, Vol. 117, No. 22, 2016, p. 225003.

[19] Parra, F., Ahedo, E., Fife, M., and Martínez-Sánchez, M., "A two-dimensional hybrid model of the Hall thruster discharge," *Journal of Applied Physics*, Vol. 100, 2006, p. 023304.

[20] Domínguez-Vázquez, A., Zhou, J., Sevillano-González, A., Fajardo, P., and Ahedo, E., "Analysis of the electron downstream boundary conditions in a 2D hybrid code for Hall thrusters," 37^{th} *International Electric Propulsion Conference*, Electric Rocket Propulsion Society, Boston, MA, June 19-23, 2022.

[21] Morozov, A., Esipchuk, Y., Tilinin, G., Trofimov, A., Sharov, Y., and G.Y.Shchepkin, "Plasma accelerator with closed electron drift and extended acceleration zone," *Soviet Physics-Tech. Physics*, Vol. 17, No. 1, 1972, pp. 38–45.

[22] Fife, J. M., "Hybrid-PIC modeling and electrostatic probe survey of Hall thrusters," Ph.D. thesis, Massachusetts Institute of Technology, 1998.

[23] Malone, R. C., McCrory, R. L., and Morse, R. L., "Indications of strongly flux-limited electron thermal conduction in laser-target experiments," *Physical Review Letters*, Vol. 34, No. 12, 1975.

[24] Stangeby, P., Canik, J., and Whyte, D., "The relation between upstream density and temperature widths in the scrape-off layer and the power width in an attached divertor," *Nuclear fusion*, Vol. 50, 2010, p. 125003.

[25] Zhou, J., Sánchez-Arriaga, G., and Ahedo, E., "Time-dependent expansion of a weakly-collisional plasma beam in a paraxial magnetic nozzle," *Plasma Sources Science and Technology*, Vol. 30, No. 4, 2021, p. 045009. https://doi.org/10.1088/1361-6595/abeff3.

[26] Marín-Cebrián, A., Domínguez-Vázquez, A., Fajardo, P., and Ahedo, E., "Macroscopic plasma analysis from 1D-radial kinetic results of a Hall thruster discharge," *Plasma Sources Science and Technology*, Vol. 30, No. 11, 2021, p. 115011. https://doi.org/10.1088/1361-6595/ac325e, URL https://doi.org/10.1088/1361-6595/ac325e.

[27] Cichocki, F., Navarro-Cavallé, J., Modesti, A., and Ramírez Vázquez, G., "Magnetic Nozzle and RPA Simulations vs. Experiments for a Helicon Plasma Thruster Plume," *Frontiers in Physics*, Vol. 10, 2022. https://doi.org/10.3389/fphy.2022.876684, URL https://www.frontiersin.org/article/10.3389/fphy.2022.876684.

[28] Merino, M., Cichocki, F., and Ahedo, E., "A collisionless Plasma thruster plume expansion model," *Plasma Sources Science and Technology*, Vol. 24, No. 3, 2015, p. 035006. https://doi.org/10.1088/0963-0252/24/3/035006.

[29] Merino, M., and Ahedo, E., "Plasma detachment in a propulsive magnetic nozzle via ion demagnetization," *Plasma Sources Science and Technology*, Vol. 23, No. 3, 2014, p. 032001. https://doi.org/10.1088/0963-0252/23/3/032001.

[30] Ahedo, E., and Merino, M., "Two-dimensional plasma expansion in a magnetic nozzle: separation due to electron inertia," *Physics of Plasmas*, Vol. 19, No. 8, 2012, p. 083501.

[31] Ahedo, E., and Merino, M., "Two-dimensional supersonic plasma acceleration in a magnetic nozzle," *Physics of Plasmas*, Vol. 17, No. 7, 2010, p. 073501.

[32] Takahashi, K., Chiba, A., Komuro, A., and Ando, A., "Experimental identification of an azimuthal current in a magnetic nozzle of a radiofrequency plasma thruster," *Plasma Sources Sci. Technol.*, Vol. 25, No. 5, 2016, p. 055011. https://doi.org/10.1088/0963-0252/25/5/055011, URL https://doi.org/10.1088/0963-0252/25/5/055011.

[33] Zhang, Y., Charles, C., and Boswell, R., "Thermodynamic study on plasma expansion along a divergent magnetic field," *Physical review letters*, Vol. 116, No. 2, 2016, p. 025001.

[34] Vinci, A., Delavière-Delion, Q., and Mazouffre, S., "Electron thermodynamics along magnetic nozzle lines in a helicon plasma," *Journal of Electric Propulsion*, Vol. 1, No. 4, 2022.